Supplementary Information for

Resource limitation modulates the fate of dissimilated nitrogen in a dual-pathway

Actinobacterium

David C. Vuono, Robert W. Read, James Hemp, Benjamin W. Sullivan, John A. Arnone III, Iva

Neveux, Bob Blank, Carl Staub, Evan Loney, David Miceli, Mari Winkler, Romy Chakraborty,

David A. Stahl, Joseph J. Grzymski

Joseph Grzymski
Email: Joe.Grzymski@dri.edu

This PDF file includes:

Supplementary Introduction
Supplementary Materials and Methods
Supplementary Results
Supplementary Discussion
Figs. S1 to S8
Tables S1 to S5
SI reference citations

SI Introduction

Dual-pathway respiratory nitrite reducers, where respiratory ammonification and denitrification

modules are encoded in the same genome, provide a unique system to investigate the molecular

mechanisms of $C:NO_3^-$ control on pathway selection as they blend the presumptively ancient

(NrfA) and modern (NirK) N-reducing modules. While many dual-pathway denitrifiers and

respiratory ammonifiers have been identified (many of which use LP ETCs), most still lack

phenotypic characterization[21–23]. Only *Shewanella loihica* PV-4, a Gram-negative, *γ*-

proteobacterium that uses UQ and dimethylmenaquinone (DMK)-based bioenergetics has been

thoroughly characterized[3, 24, 43]. Nonetheless, these dual-pathway nitrite reducers are capable

of differential energy conservation through pathway bifurcation of nitrite. Yet no mechanistic or

metabolic models exist to explain how these dual-pathway organisms partition electron flow and

proton translocation between pathways to maximize resource-use efficiency. It is not known if

these organisms differentially distribute electron flow through alternative respiratory chains in

650 response to shifting resource availability or control each pathway independently in response to

651 resource thresholds. Is there an evolutionary and biochemical basis for pathway selection?

652 It has long been postulated that $C:NO_3^-$ ratio modulates the activity of respiratory

653 ammonification versus denitrification[2], with numerous studies in recent years differing in the

654 methods used to calculate $C:NO_3^-$ ratio, carbon sources used, range of C:N ratios tested,

655 magnitudes of C and N concentrations, sample types (enrichment cultures vs isolates), and

656 culturing mode (chemostat/batch culture) (Table S4)[3–6, 34]. The hypothesis for $C:NO_3^-$

657 control states that high $C:NO_3^-$ ratios (stoichiometric limitation of nitrate relative to C) drive

658 respiratory ammonification while low $C:NO_3^-$ ratios (stoichiometric limitation of C relative to

659 nitrate) drive denitrification. This hypothesis is based on the rationale that denitrification

660 theoretically yields more free energy per electron, but respiratory ammonification yields more

661 free energy per nitrate due to the stoichiometry of each reaction: one nitrate is needed to make

662 ammonium while two are needed to make N_2O/N_2[2, 39]. Thus, when $C:NO_3^-$ ratio is low, cells

663 select denitrification to maximize the free energy advantage per electron. When $C:NO_3^-$ is high,

664 cells select respiratory ammonification to maximize the free energy advantage per nitrate.

665 However, the theoretical basis for this prediction is inconsistent with the observation that growth

666 yields of pure denitrifiers are significantly lower than expected and lower than growth yields of

667 respiratory ammonification[39]. This observation suggests that despite a lower free energy yield

668 (ΔG) compared to denitrification, respiratory ammonification conserves more energy during

669 catabolism, through the generation of a proton motive force (Δp) in the ETC, to build more

670 biomass during anabolism. Thus, there is a need to better understand the effects of different

671 nutrient limitations on growth and pathway selection (i.e., allocation of C and N to dissimilatory

672 and assimilatory processes), which are often confounded by $C:NO_3^-$. For example, reportedly

673 "low" $C:NO_3^-$ ratios rarely fall below 1.5 have rarely been tested (Table S4), conditions in which

674 C would be a growth-limiting resource. Instead, pathway selection should be better predicted by

675 1) Liebig's law of the minimum (LM) and 2) the maximum power principle (MPP)[37]. Under

676 the MPP, which states that biological systems are designed to maximize power intake and energy

677 transformation, the cell's aim is therefore to maximize power (i.e., realized in the form of growth

678 rate and yield) given the constraints of a growth-limiting nutrient (i.e., LM). Therefore, limitation

679 of a growth-limiting nutrient, whether it be C or NO_3^-, should dictate the selection of the most

680 efficient respiratory module to maximize power (i.e., MPP).

681 **SI Materials and Methods**

682 <u>Sample collection</u>: *I. calvum* was isolated from a groundwater well (GW247) collected on

683 2/18/2013 at Oak Ridge National Laboratory (Lat: 35.97990, Long: 84.27059) with a

684 groundwater temperature of 15.57 ºC, conductivity of 521.9 µS/cm, and pH of 7.71. *I. calvum*

685 was isolated and obtained from Dr. R. Chakraborty (Lawrence Berkeley National Laboratory).

686 We began our experimental process by first picking single colonies from LB agar plates and

687 transferring the clonal isolates to LB broth.

688 <u>Media preparation</u>: Media preparation was conducted in a 2L Widdel Flask. After autoclaving,

689 the media was immediately put under an anoxic headspace (N2/CO2 80:20 mix) and sterile

690 filtered (0.2µm) trace elements, trace vitamins, and reducing agent were added. The media was

691 cooled under an anoxic headspace and buffered with bicarbonate to maintain a pH of 7.2.

692 Hungate technique was used to dispense media into culture tubes (20 mL) and serum vials (100

693 mL) pre-flushed with a sterile stream of ultra-high purity (UHP) N_2 and sealed with blue 1" butyl

694 rubber stoppers. End-point cultures were grown in Balch tubes (18x150-mm glass tube) sealed

695 with butyl rubber stoppers. Cultures for time-course sampling were grown in 160ml serum vials.

696 All end-point experiments were terminated after 100 hours unless otherwise noted.

697 <u>Growth Curve/Cell counts/Yield Measurements</u>: Growth curves were measured from scratch-

698 free Balch-tubes grown cultures using an automated optical density reader at OD_{600} nm

699 (Lumenautix LLC, Reno, NV). End-point cultures were monitored until all replicates reached

700 stationary phase (65-100 hours depending on $C:NO_3^-$ treatment) (Figure S6).

701 Cell counts were performed by fixing cells in 4% paraformaldehyde (final concentration) for 20

702 minutes, filtered onto 0.2µm pore-sized black polycarbonate filters, and washed three times with

703 phosphate buffered saline (PBS, pH 7.2). Filtered cells captured on the black polycarbonate

704 filters were stained with SYBR® Gold nucleic acid stain (10-minute incubation) (ThermoFisher

705 Scientific) and counted manually with a fluorescence microscope (Olympus BX60, Tokyo,

706 Japan). We collected cells from during lag phase, exponential phase, and stationary phase in

707 order to create a standard curve of cell counts versus optical density (OD_{600}). We fit a linear

708 model to cell count versus OD_{600} (R^2=0.99) and used the resulting linear equation for cell count

709 enumeration for growth curves during our various treatment conditions.

710 Biomass concentrations were measured by filtration and drying as per standard protocol [26] for

711 8mM lactate/12mM nitrate and 0.8mM lactate/1.2mM nitrate treatments and conducted in

712 parallel with growth curve/cell counts as described above. Analysis from triplicate cultures

713 yielded (0.064 ± 0.003) and (0.016 ± 0.001) mg of biomass (dry weight) ml^{-1} for 8mM and 0.8

714 mM lactate cultures, respectively. Cell counts from stationary phase cultures were (1.5 ± 0.05) x

715 10^7 and (1.16 ± 0.09) x 10^6 for 8mM and 0.8 mM lactate cultures, respectively. From these

716 values the dry weight of a single *I. calvum* cell was estimated to be 1.09 x 10^{-10} g. Growth yield

717 (*Y*) (Table S3) was calculated by dividing biomass (g) by lactate mass (g) and moles consumed,

718 as described by [56]. Lactate measurements are described below.

719 Thermodynamic calculations for anaerobic lactate oxidation with nitrate and nitrite were carried

720 out using standard Gibbs free-energy values defined by Thauer *et al*., [57].

721 <u>Ion and Gas Chromatography Measurements</u>: New glass IC vials were used for every sample in

722 order to ensure no cross contamination of analytes. Ammonium production via respiratory nitrite

723 ammonification was measured as described by [24]. Briefly, because the bacterium

724 simultaneously produces (via dissimilation) and consumes (via assimilation) ammonium,

725 ammonium consumption was first measured with O_2 and lactate by calculating the difference

726 between starting and ending ammonium concentrations. These ammonium consumption values

727 were then normalized to lactate consumed $(0.31\mu mols\ NH_4^+/lactate)$ $(7.07x10^{-7}\mu mols\ NH_4^+/cell$

728 calculated from average cell number of stationary phase biomass; Figure S6). Ammonium

729 production during nitrate reducing conditions was then calculated using the mass balance

730 approach from [58] for Total Belowground Carbon Allocation (TBCA) but adapted for nitrogen

731 flux instead of carbon flux:

732 $$\Delta NH_4^+ = (\Delta lactate_{start-end} \text{ x } 0.31\mu mols\ NH_4^+/lactate) + \Delta NH_4^+{}_{end-start} \qquad (1)$$

733 Here, the $\Delta lactate_{start-end}$ variable (µmols) is multiplied by the ammonium consumed per lactate

734 consumed constant. This value is added to the $\Delta NH_4^+{}_{end-start}$ variable (µmols), denoted as ending

735 minus starting concentration, which defines whether the change in ammonium is positive (more

736 ammonium produced than consumed) or negative (more ammonium consumed than produced).

737 Headspace gas from Balch tubes and serum vials was sampled with volume appropriate gastight

738 syringes (Hamilton Company, Reno, NV) pre-flushed with UHP N_2. For high and low nutrient

739 treatments, 10μl and 100μl of headspace were sampled and diluted into 12ml exetainters (Labco,

740 Lampter, Wales, UK) over-pressurized with 15ml UHP N_2, respectively. Similar dilutions were

741 performed for nitrite as e-acceptor experiments, ammonium-deplete experiments, and time-series

742 experiments. For time-series experiments, an equal volume of headspace gas that was removed at

743 each time-point was replaced with sterile UHP N_2. N_2O and NO were measured by gas

744 chromatography (Shimadzu Greenhouse Gas Analyzer GC-2014) using a 500μl injection

745 volume. The rubber septa on the injection port of the GC was replaced after 100 injections in

746 order to prevent leakage of the sample after the injection needle was lifted out from the injection

747 port. Aqueous concentrations of N_2O were calculated using a Henry's constant of 1.751 (mM

748 (g)/mM (aq)) corrected for the medium's ionic strength and temperature. A total of 8-11

749 replicates per treatment were analyzed for all experiments discussed in this work (Table S5).

750 Phylogenetic, Genomic, and Transcriptomic Analysis: A set of 34 NrfA amino acid sequences,

751 representing 33 complete genome sequences and 1 octaheme nitrite reductase (ONR) from

752 known respiratory ammonification organisms were downloaded from GenBank (Table S1). A

753 multiple sequence alignment (MSA) was generated from the sequences annotated as cytochrome

754 c nitrite reductase and ONR using MUSCLE [59]. The resulting alignment was visualized within

755 MEGA5 [60] where the alignment was manually screened for the presence of conserved amino

756 acid residues consistent with those found in NrfA (i.e., heme motifs). A maximum likelihood tree

757 was created from the alignment using RAxML [61] with 500 bootstrap iterations. The presence

758 of NapA, NarG, NirK, and Nor modules were manually queried from each NCBI genome in our

759 set and confirmed by MSA, as described above. Metabolic pathway for pool quinone type was

760 queried on BioCyc Pathway/Genome Database (biocyc.org) for each organism in our set. The

761 structure of *I. calvum*'s NirK protein was predicted using the protein structure predicting

762 algorithm Phyre2 [62]. Protein atomic composition for C and N was calculated from amino acid

763 sequences as input files, as described by [14, 15], using custom python scripts for each element

764 separately (github.com/dvuono/Cost_minimization).

765 Due to the high similarity of C5 to 7KIP, reads were aligned to the *Intrasporangium calvum*

766 genomic reference sequence and gtf file (Acc: NC_014830.1) using the STAR RNA-seq

767   aligner[63], with the --limitBAMsortRam parameter set to the recommended value by STAR.

768   Sequence reads were mapped to genomic features to obtain count data using featureCounts [64].

769   Systematic changes across experimental conditions were performed on normalized read counts in

770   DESeq2 [65]. The RNA-seq data reported in this study are available within the NCBI BioProject

771   number PRJNA475609.

772   **SI Results**

773   **Genomic analysis of *I. calvum* C5.** *I. calvum* C5 was isolated from a nitrate contaminated well

774   (>200mM nitrate) at the Oak Ridge National Laboratory Field Research Station in Oak Ridge,

775   TN. The strain was selected for further analysis due to its nitrate reducing phenotype in minimal

776   media. The genome consists of a 4,025,044-base pair chromosome and encodes for 3,722

777   predicted genes, 2,665 protein coding genes, 57 RNA genes, and two rRNA operons.

778   ***I. calvum* encodes for a functional NrfAH complex and assimilates NH_4^+ via respiratory**

779   **nitrite ammonification.** The potential routes for N-assimilation were screened using aerobic

780   minimal media with defined C-source/e-donor and e-acceptor, and with nitrate or ammonium as

781   assimilatory N-sources. Based on genomic information, the bacterium possesses no known

782   assimilatory nitrate reductase, but encodes for an ammonium transporter (Intca_RS11655) and

783   GS/GOGAT pathways (Intca_RS13810; Intca_RS11930; Intca_RS08335, 08340), suggesting

784   that ammonium is its sole assimilatory N source. Indeed, we observed no aerobic growth with

785   8mM lactate, O_2, and nitrate as N-source. However, when grown on 8mM lactate, O_2, and

786   1.5mM ammonium as N-source, *I. calvum* displayed a typical growth curve with a specific

787   growth rate of 0.4±0.02 μ (1.7±0.1 doublings/hour) (Figure S7).

788   **SI Discussion**

789   *S. loihica* PV-4 (a Gram-negative dual-pathway γ-proteobacterium) and *I. calvum* use different

790   types of nitrate reducing modules. *S. loihica* PV-4 utilizes NapA whereas *I. calvum* utilizes NarG

791   (Figure 1). The latter translocates two H^+ per nitrate reduced while NapA consumes two H^+ in

792   the periplasm [17]. Both reductases would generate a Δp via NADH dehydrogenase H^+

793   translocation, but the NapA module would result in a net loss of two H^+, which may impact the

794   selection of downstream respiratory modules. For example, given the lower-than-expected

795   observed growth yields of denitrifiers compared to respiratory ammonifiers [39], if a NapA

796   module is used, it would make sense for respiratory ammonification to be selected under high

797   C:N ratios because the cell would need to compensate for less energy conservation during nitrate

798   reduction. Nitric oxide reductase composition may also impact pathway selection. For example,

799   qNor does not translocate H^+, while sNor, eNor, and gNor are predicted to conserve energy

800   through H^+ translocation [41]. Thus, the modularity of dissimilatory N reduction processes, and

801   whether those modules conserve energy or not, may impose certain constraints on pathway

802   selection in different organisms and should be further investigated.

803

C:NO$_3^-$ 4 2 1.5 1 0.5 0.1

$y= 0.258x + 0.066$
$R^2 = 0.5, p < 0.001$

N fraction dissimilated by Respiratory Ammonification
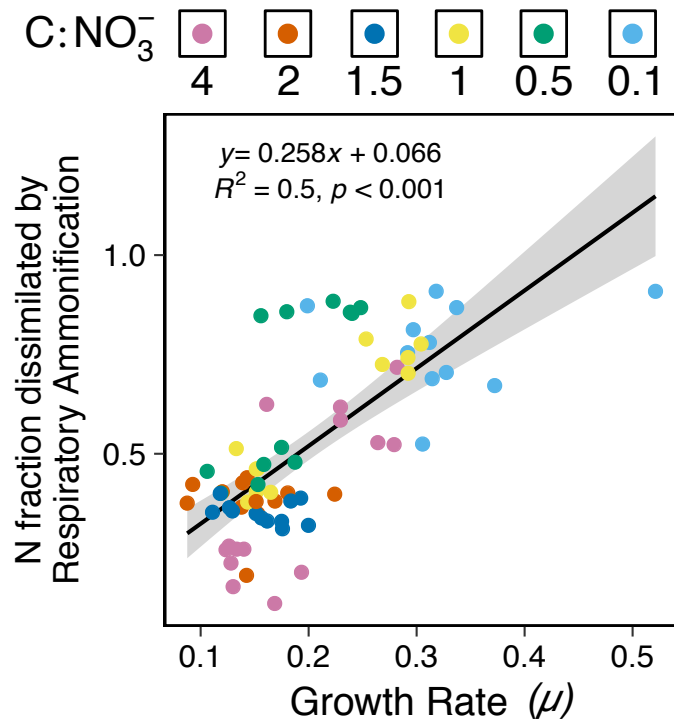
Growth Rate (*μ*)

809
810 Figure S1. Relationship between growth rate and the fraction of N dissimilated by respiratory
811 ammonification for high and low nutrient concentrations. Treatments under C and NO$_3^-$ scarcity,
812 even with low C:NO$_3^-$ ratios, disproportionately produce more ammonium and have higher
813 growth rates.
814
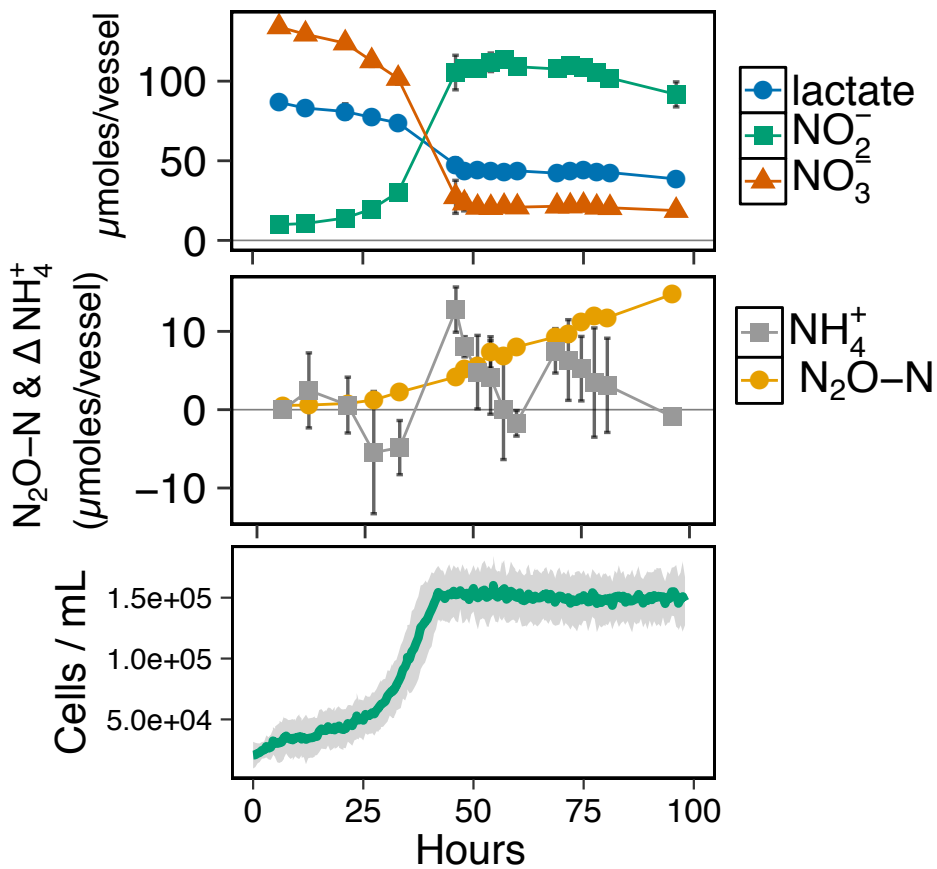
817   Figure S2. Time-series metabolite profiles of a 96-hour incubation for lactate, nitrate, and nitrite
818   (top pane), production of dissimilated end-products as N_2O-N and net change in NH_4^+
819   ammonium production (middle pane), and corresponding growth curve of *I. calvum* cells grown
820   under 0.8mM lactate 1.2mM nitrate (C:NO_3^- ratio = 2) (bottom pane).
821

822

High Nutrients
8mM Lac, 12mM NO_3^-

Low Nutrients
0.8mM Lac, 1.2mM NO_3^-
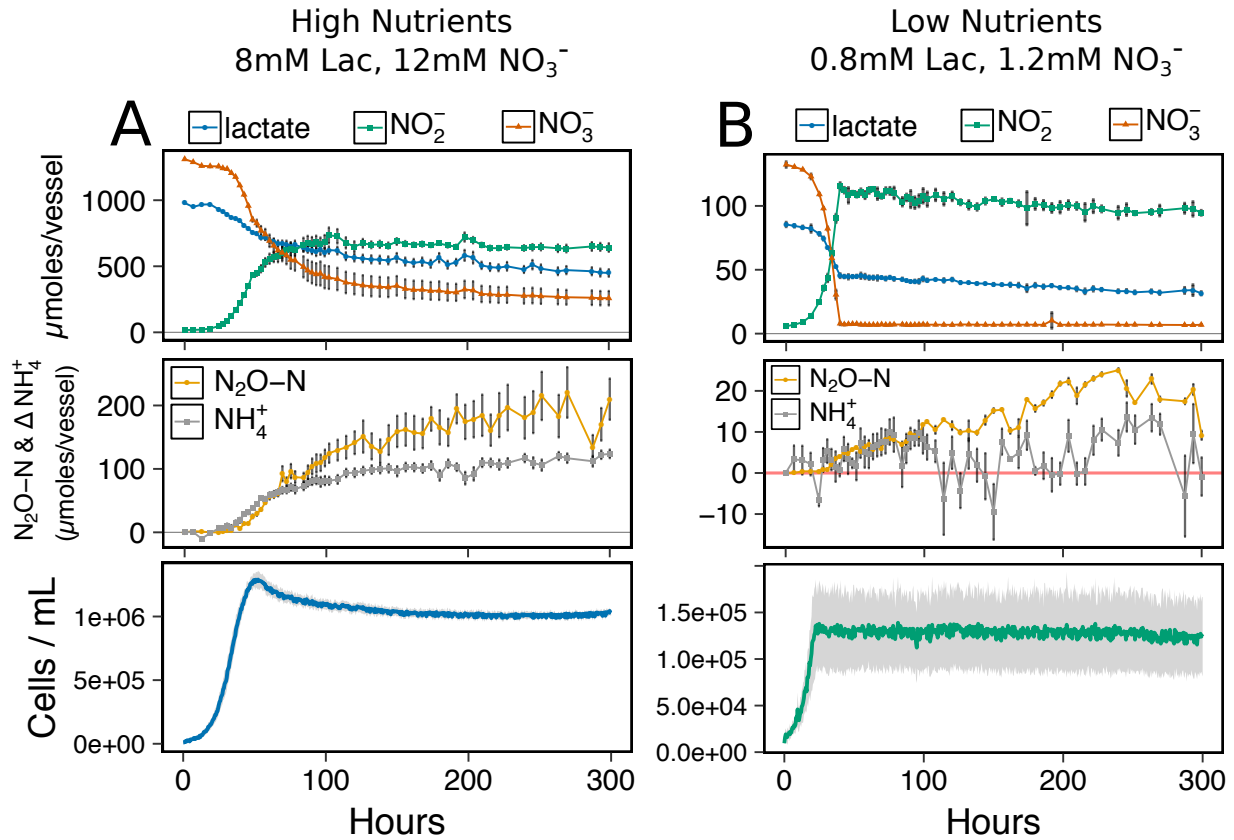
823
824 Figure S3. Time-series metabolite profiles of a 300-hour incubation for (A) high nutrient and (B)
825 low nutrient concentrations. Shown are the profiles of lactate, nitrate, and nitrite (top pane),
826 production of dissimilated end-products as N_2O-N and net change in NH_4^+ ammonium
827 production (middle pane), and corresponding growth curves of *I. calvum* cells (C:NO_3^- ratio = 2)
828 (bottom pane).

829
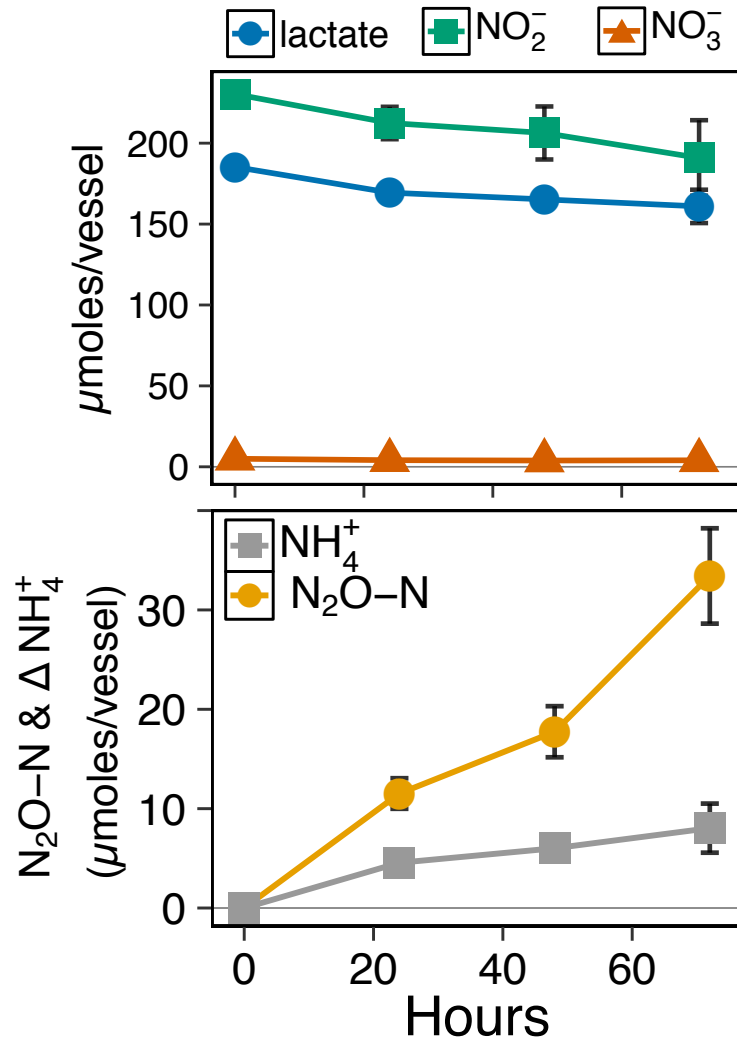
Figure S4. Time-series metabolite profiles of a 72-hour incubation conducted in balch-tubes grown under 8mM lactate 12mM nitrite (C:NO_2^- ratio = 2). Profiles for lactate and nitrite (top pane) and production of dissimilated end-products as N_2O-N and net change in NH_4^+ ammonium production (bottom pane).
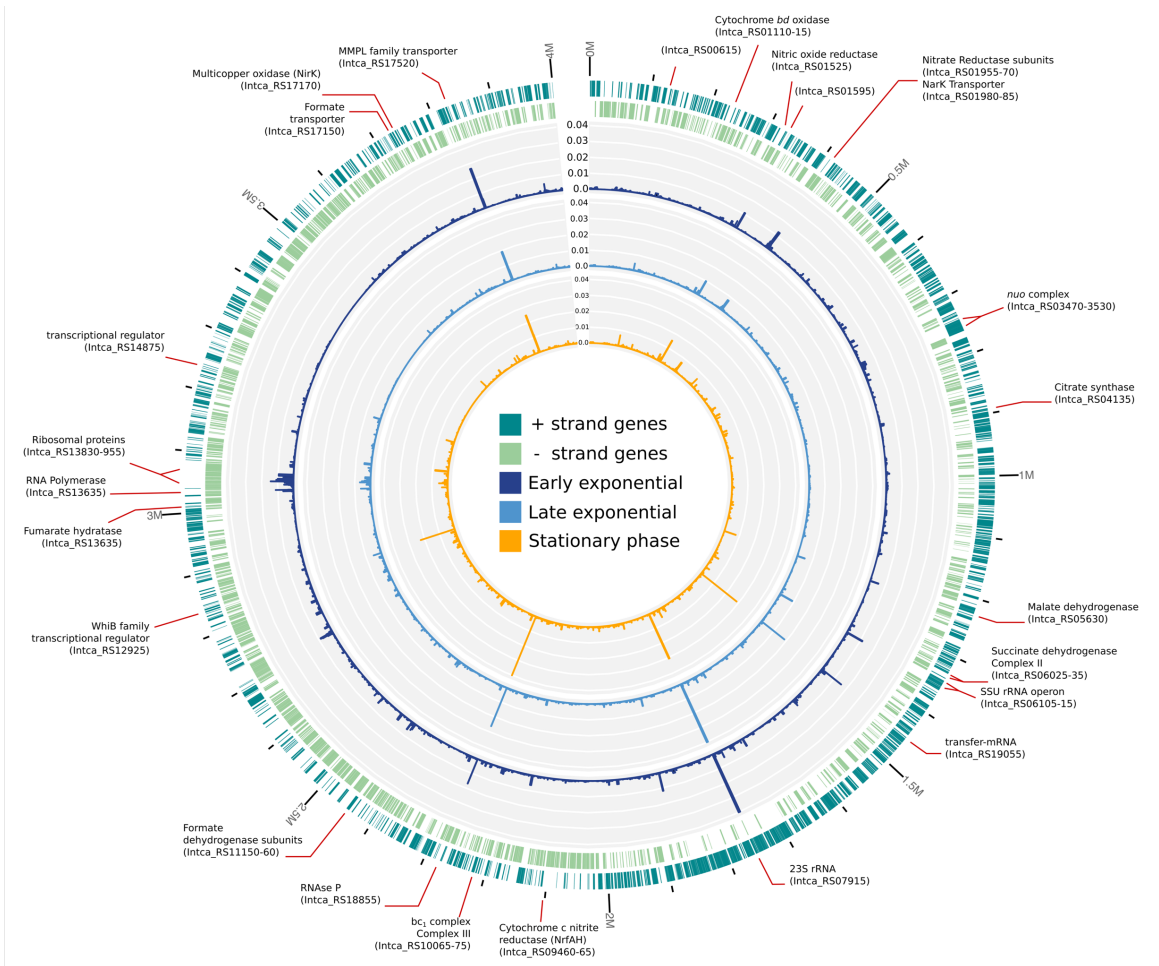
Figure S5. The genome-wide transcriptional changes of early exponential, late exponential, and stationary phase *I. calvum* cells. The first and second outermost rings (dark and light green indicate the open reading frames (ORFs) on the positive and negative strands. The third, fourth, and fifth rings are the relative abundance of transcripts mapped onto the *I. calvum* genome based on the transcript read counts from early exponential phase, late exponential phase and stationary phase, respectively. The position and locus IDs are marked for the most highly expressed genes and genes involved in the ETC.

845

846

847

848
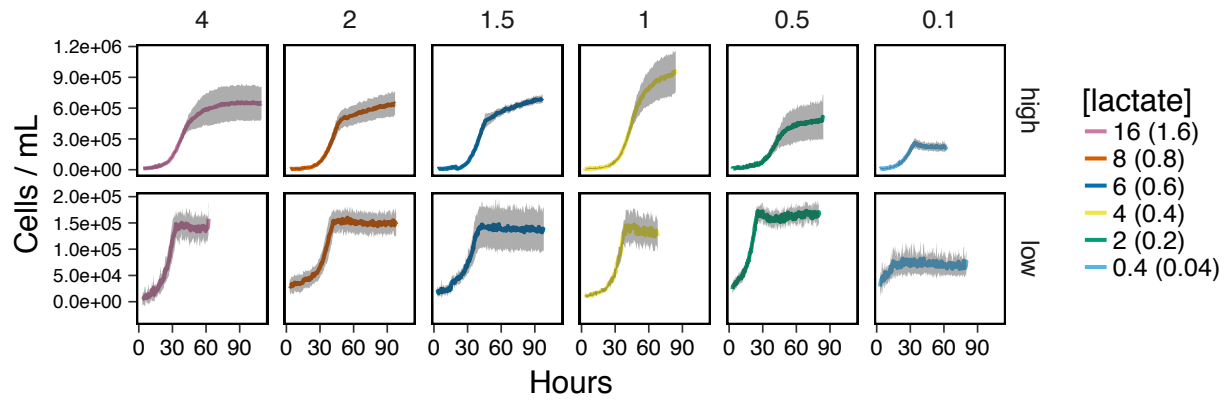
849 Figure S6. Mean cell concentrations for I. calvum cultures grown over a range of C:NO$_3^-$ ratios

850 (columns) at high nutrient (top row) and low nutrient (bottom row) concentrations of the same

851 ratio. Each growth curve consists of n=6 replicates.

852

853
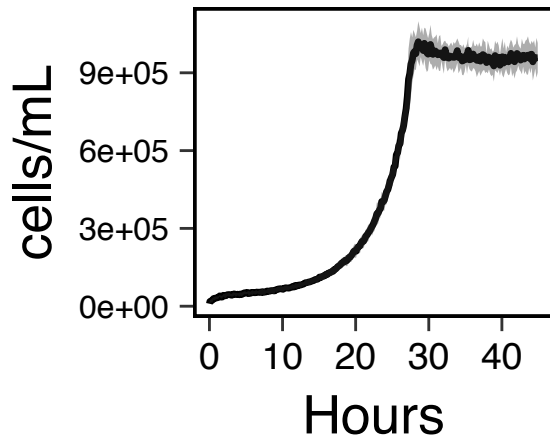
854
855 Figure S7. Growth curve of *I. calvum* in a sealed Balch-tube with lactate and O_2 as electron
856 donor/acceptor pair and with ammonium as sole nitrogen source.

857

Table S1. Organism accession numbers for NrfA and NirK modules.

Organisms	Accession #
	NrfA
Escherichia_coli_K-12	NC_000913.3
Salmonella_enterica CT18	NC_003198.1
Yersinia_kristensenii	NZ_CP009997.1
Yersinia_frederiksenii	NZ_CP009364.1
Vibrio fischeri_ES114	NC_006840.2
S._loihica-PV-4	NC_009092.1
Shewanella_oneidensis_MR-1	NC_004347.2
Desulfotalea_psychrophila_LSv54	NC_006138.1
Sulfurospirillum_deleyianum	NC_013512.1
Wolinella_succinogenes	NC_005090.1
Flexibacter_tractuosus	NC_014759.1
Porphyromonas_gingivalis_W83	NC_010729.1
Symbiobacterium_thermophilum	NC_006177.1
Carboxydothermus_hydrogenoformans	NC_007503.1
Desulfovibrio_vulgaris_Hildenborough	NC_002937.3
Bacillus_vireti	NZ_LDNB01000003.1
Bacillus_bataviensis	NZ_AJLS01000002.1
Bacillus_azotoformans	NZ_AJLR01000001.1
Bacillus_selenitireducens_MLS10	NC_014219.1
Campylobacter_jejuni	NC_002163.1
Opitutus_terrae	NC_010571.1
Anaeromyxobacter_dehalogenans_2_CP-1	NC_011891.1
Rhodopirellula_baltica	NC_005027.1
Intrasporangium calvum 7KIP	NC_014830.1
Intrasporangium calvum C5	This study
Bdellovibrio_bacteriovorus	NC_005363.1
Gimesia_maris	NZ_ABCE01000001.1
Candidatus_Nitrospira_inopinata	NZ_LN885086.1
Myxococcus_xanthus	NC_008095.1
Geobacter_metallireducens_GS_15	NC_007517.1
Geobacter_sulfurreducens_PCA	NC_002939.5
Thioalkalivibrio_nitratireducens	NC_019902.2
Thermodesulfovibrio_yellowstonii_THEYE_A0193	NC_011296.1
	NirK
multicopper_oxidase_[Intrasporangium_calvum]	WP_013494195.1
nitrite_reductase,_copper-containing_[Shewanella_loihica]	WP_011867131.1
nitrite_reductase_[Candidatus_Nitrospira_inopinata]	WP_062488124.1
nitrite_reductase,_copper-containing_[Marivirga_tractuosa]	WP_013454821.1
nitrite_reductase,_copper-containing_[Symbiobacterium_thermophilum]	WP_070105442.1
nitrite_reductase_[Opitutus_terrae]	WP_012373845.1

nitrite_reductase,_copper-containing_[Bdellovibrio_bacteriovorus]	WP_011165004.1
Nitrite_reductase_OS=Bacillus_azotoformans_GN=nirK	ZP_08007035.1
Ochrobactrum_anthropi_ATCC_49188	NC_009668.1
Bradyrhizobium_japonicum_USDA_110	NC_004463.1
Agrobacterium_fabrum_str._C58	NC_003063.2
Sinorhizobium_meliloti_1021	NC_003037.1
Pseudomonas_citronellolis_strain_SJTE-3	NZ_CP015878.1
Rhodanobacter_denitrificans_strain_2APBS1	NC_020541.1
Taylorella_equigenitalis_ATCC_35865	NC_018108.1
Flavobacterium_columnare_ATCC_49512	NC_016510.2
Actinobacillus_suis_ATCC_33415	NZ_CP009159.1
Chromobacterium_violaceum_ATCC_12472	NC_005085.1
Halopiger_xanaduensis_SH-6	NC_015666.1
Halopiger_xanaduensis_SH-6	NC_015666.1
inorhizobium_fredii_HH103	NC_016812.1
Pseudomonas_entomophila_str._L48	NC_008027.1
Pseudomonas_denitrificans_ATCC_13867	NC_020829.1
Flavobacterium_johnsoniae_UW101	NC_009441.1
Rhizobium_etli_CFN_42	NC_007766.1
Ochrobactrum_anthropi_ATCC_49188	NC_009667.1
Caulobacter_segnis_ATCC_21756	NC_014100.1
Rhizobium_giardinii_bv._giardinii_H152	NZ_KB902685.1

Table S2. Concentration and ratio experimental design and produciton values for NH_4^+ and N_2O-N.

[C] (mM)	[NO3] (mM)	C:NO3- ratio	Ammonia per Cell NH4 produced (µmoles)	Ammonia per Lactate NH4 produced (µmoles)	N_2O produced (µmoles)	% Recovery of Dissimilated N
16	12	4	1.94 ± 1.31	7.79 ± 3.3	27.4 ± 7.5	91.64 ± 12.9
8	12	2	4.91 ± 1.07	10.8 ± 4.1	18.1 ± 6.7	72.87 ± 9.3
6	12	1.5	3.07 ± 4.50	10.2 ± 3.8	19.1 ± 6.2	72.77 ± 4.1
4	12	1	8.06 ± 2.19	14.5 ± 4.2	18.1 ± 6.8	61.79 ± 5.1
2	12	0.5	3.82 ± 1.92	8.76 ± 2.9	10.2 ± 3.7	64.21 ± 9.8
0.4	12	0.1	2.05 ± 0.50	1.55 ± 0.2	0.48 ± 0.1	24.44 ± 7.5
1.6	1.2	4	1.12 ± 0.99	2.39 ± 0.7	1.77 ± 0.2	70.47 ± 10.4
0.8	1.2	2	1.50 ± 0.57	2.32 ± 0.5	3.72 ± 0.4	90.71 ± 8.2
0.6	1.2	1.5	0.90 ± 0.53	2.27 ± 0.5	4.53 ± 0.7	88.31 ± 8.6
0.4	1.2	1	1.18 ± 1.17	2.45 ± 0.3	0.88 ± 0.3	50.20 ± 9.4
0.2	1.2	0.5	1.91 ± 0.33	1.13 ± 0.2	0.18 ± 0.0	43.34 ± 20.0
0.04	1.2	0.1	0.03 ± 0.95	0.28 ± 0.2	0.06 ± 0.0	18.10 ± 10.9

Table S3. Growth rate and growth yield values for concentration and ratio experiment.

[C] (mM)	[NO3] (mM)	C:NO3- ratio	Specific Growth Rate (μ)	Doubling Time (hours/generation)	Growth Yield cells (g)/Lac(g)	Molar Growth Yield cells (g)/moles Lac	Growth Yield cells (g)/NO3(g)	Molar Growth Yield cells (g)/moles NO3	Growth Yield cells (g)/NO2(g)	Molar Growth Yield cells (g)/moles NO2
			n=6	n=6	n=3	n=3	n=3	n=3	n=3	n=3
16	12	4	0.143 ± 0.02	4.96 ± 0.73	0.25 ± 0.05	22.3 ± 4.6	0.10 ± 0.02	6.43 ± 1.23	0.63 ± 0.19	28.8 ± 8.6
8	12	2	0.144 ± 0.02	4.86 ± 0.55	0.29 ± 0.02	26.4 ± 1.4	0.12 ± 0.03	7.61 ± 1.77	0.66 ± 0.21	30.1 ± 9.6
6	12	1.5	0.150 ± 0.03	4.77 ± 0.94	n.a.	n.a.	0.11 ± 0.02	6.84 ± 1.45	0.62 ± 0.21	28.6 ± 9.5
4	12	1	0.150 ± 0.01	4.65 ± 0.34	0.26 ± 0.11	23.5 ± 9.6	0.12 ± 0.05	7.46 ± 2.79	0.62 ± 0.25	28.5 ± 11.3
2	12	0.5	0.150 ± 0.03	4.82 ± 1.12	0.27 ± 0.02	24.3 ± 2.2	0.10 ± 0.03	6.38 ± 1.88	0.58 ± 0.18	26.7 ± 8.1
0.4	12	0.1	0.290 ± 0.05	2.46 ± 0.51	0.46 ± 0.003	41.1 ± 0.27	0.15 ± 0.01	9.41 ± 0.66	0.92 ± 0.20	42.5 ± 9.4
1.6	1.2	4	0.241 ± 0.05	2.98 ± 0.69	0.26 ± 0.03	23.5 ± 3.1	0.11 ± 0.01	6.86 ± 0.72	0.83 ± 0.05	38.32 ± 2.48
0.8	1.2	2	0.146 ± 0.05	5.31 ± 1.96	0.29 ± 0.02	25.7 ± 2.2	0.11 ± 0.00	6.99 ± 0.01	0.78 ± 0.06	36.07 ± 2.93
0.6	1.2	1.5	0.164 ± 0.03	4.39 ± 0.97	0.23 ± 0.02	20.8 ± 2.3	0.10 ± 0.00	6.47 ± 0.02	0.63 ± 0.09	29.06 ± 4.20
0.4	1.2	1	0.284 ± 0.02	2.45 ± 0.17	0.27 ± 0.01	23.9 ± 0.5	0.10 ± 0.00	6.51 ± 0.03	0.73 ± 0.09	33.72 ± 4.16
0.2	1.2	0.5	0.214 ± 0.04	3.33 ± 0.67	0.57 ± 0.01	51.4 ± 0.6	0.12 ± 0.00	7.67 ± 0.19	n.a.	n.a.
0.04	1.2	0.1	0.344 ± 0.10	2.16 ± 0.64	n.a.	n.a.	n.a.	n.a.	n.a.	n.a.

Table S4. Literature summary of C:N ratio controls on N dissimilation.

Citation	C-source	C:N range	C conc range	NO3 conc range	units	calc method
Kraft *et al.* 2014 (17)	amino acids	1.5-3	4.4-43.5	0.5-14.4	mmol	mmol-C/mmol-$\sum NO_x$
Yoon et al. 2015 (3)	lactate	1.5-150	0.1-10	0.2	mM	nC*mM-C/nN*mM-N
Van den Berg et al. 2015 (4)	acetate	1.8-7.7	160-595	82-93	mg/L	mg-COD/mg-N
Schmidt et al. 2011 (5)	Soil organic-C	not specified	2.7-11.4	22.4-79.8	C%,mg-N/kg soil	not specified
Hardison et al. 2015 (6)	complex	not specified	C+ - C-	0.6-5	µg	not specified
Fazzolari et al. 1998 (7)	glucose	2.5-10	250-1000	100	mg/kg dried soil	mg-C/mg-N
This study	lactate	0.1-4	0.004-16	1.2-12	mM	nC*mM-C/nN*mM-N

Table S5. Summary of all experimental conditions and replicate number in the current study (Figure 2 in main text).

NO_3^- (mM)	Lactate (mM)	Ratio $C:NO_3^-$	experiment type	ammonium-deplete	replicates	Number of samples taken
1.2	0.04	0.1	end-point	n	9	2
1.2	0.2	0.5	end-point	n	9	2
1.2	0.4	1.0	end-point	n	10	2
1.2	0.6	1.5	end-point	n	10	2
1.2	0.8	2.0	end-point	n	9	2
1.2	1.6	4.0	end-point	n	10	2
12	0.4	0.1	end-point	n	10	2
12	2	0.5	end-point	n	8	2
12	4	1.0	end-point	n	8	2
12	6	1.5	end-point	n	10	2
12	8	2.0	end-point	n	10	2
12	16	4.0	end-point	n	8	2
12	8	2.0	time-series	n	3	17
1.2	0.8	2.0	time-series	n	3	17
12	8	2.0	time-series	n	3	59
1.2	0.8	2.0	time-series	n	3	59
12*	8	2.0	time-series	n	11	4
12	8	2.0	time-series	y	10	3

*nitrite is used as the electron acceptor